AFRL-AFOSR-VA-TR-2018-0413

Pulsed Microwave Plasma Instrumentation for Investigation of Plasma-Tuned Multiphase Combustion

Travis Sippel
IOWA STATE UNIVERSITY
1350 BEARDSHEAR HALL
AMES, IA 50011

11/13/2018
Final Report

Air Force Research Laboratory
AF Office Of Scientific Research (AFOSR)/RTA1
Arlington, Virginia 22203 Air Force Materiel Command

REPORT DOCUMENTATION PAGE

Form Approved
OMB No. 0704-0188

1. REPORT DATE *(DD-MM-YYYY)*	2. REPORT TYPE	3. DATES COVERED *(From - To)*
10/21/2018	Final Report	10/2015-10/2016

4. TITLE AND SUBTITLE

Pulsed Microwave Plasma Instrumentation for Investigation of Plasma-Tuned Multiphase Combustion

5a. CONTRACT NUMBER

5b. GRANT NUMBER

FA9550-15-1-0195

5c. PROGRAM ELEMENT NUMBER

6. AUTHOR(S)

Travis Sippel, James Michael, Stuart Barkley, Keke Zhu

5d. PROJECT NUMBER

5e. TASK NUMBER

5f. WORK UNIT NUMBER

7. PERFORMING ORGANIZATION NAME(S) AND ADDRESS(ES)

Iowa State University
Department of Mechanical Engineering
Ames, IA 50011

8. PERFORMING ORGANIZATION REPORT NUMBER

9. SPONSORING/MONITORING AGENCY NAME(S) AND ADDRESS(ES)

USAF, AFRL
AF OFFICE OF SCIENTIFIC RESEARCH
875 NORTH RANDOLPH STREET, RM 3112 ARLINGTON VA 22203-1954

10. SPONSOR/MONITOR'S ACRONYM(S)

AFOSR

11. SPONSOR/MONITOR'S REPORT NUMBER(S)

12. DISTRIBUTION/AVAILABILITY STATEMENT

DISTRIBUTION A. Approved for public release: distribution unlimited.

13. SUPPLEMENTARY NOTES

The views, opinions and or findings contained in this report are those of the author (s) and should not contrued as an official USAF position, policy or decision, unless so designated by other documentation

14. ABSTRACT

This report describes the twelve month Iowa State University effort on the topic of exploration of strategies to dynamically co ntrol the combustion of a composite solid propellant flame through energy deposition of microwave frequency radiation to pr opellant flame structures. Specifically, techniques to enhance burning rate focus on two techniques: (1) microwave supporte d plasma flame enhancement and (2) energy deposition to condensed phase flame features having 'thermal runaway' micro wave energy absorption characteristics. Burning rate enhancements of ~20-30% are achieved with relatively low power inpu

15. SUBJECT TERMS

composite solid propellant, burning rate control, plasma, alkali metal

16. SECURITY CLASSIFICATION OF:			17. LIMITATION OF ABSTRACT	18. NUMBER OF PAGES	19a. NAME OF RESPONSIBLE PERSON
a. REPORT	b. ABSTRACT	c. THIS PAGE			Travis Sippel
UU	UU	UU	UU	44	19b. TELEPHONE NUMBER *(Include area code)* 515-294-3803

INSTRUCTIONS FOR COMPLETING SF 298

1. REPORT DATE. Full publication date, including day, month, if available. Must cite at least the year and be Year 2000 compliant, e.g. 30-06-1998; xx-06-1998; xx-xx-1998.

2. REPORT TYPE. State the type of report, such as final, technical, interim, memorandum, master's thesis, progress, quarterly, research, special, group study, etc.

3. DATE COVERED. Indicate the time during which the work was performed and the report was written, e.g., Jun 1997 - Jun 1998; 1-10 Jun 1996; May - Nov 1998; Nov 1998.

4. TITLE. Enter title and subtitle with volume number and part number, if applicable. On classified documents, enter the title classification in parentheses.

5a. CONTRACT NUMBER. Enter all contract numbers as they appear in the report, e.g. F33315-86-C-5169.

5b. GRANT NUMBER. Enter all grant numbers as they appear in the report. e.g. AFOSR-82-1234.

5c. PROGRAM ELEMENT NUMBER. Enter all program element numbers as they appear in the report, e.g. 61101A.

5e. TASK NUMBER. Enter all task numbers as they appear in the report, e.g. 05; RF0330201; T4112.

5f. WORK UNIT NUMBER. Enter all work unit numbers as they appear in the report, e.g. 001; AFAPL30480105.

6. AUTHOR(S). Enter name(s) of person(s) responsible for writing the report, performing the research, or credited with the content of the report. The form of entry is the last name, first name, middle initial, and additional qualifiers separated by commas, e.g. Smith, Richard, J, Jr.

7. PERFORMING ORGANIZATION NAME(S) AND ADDRESS(ES). Self-explanatory.

8. PERFORMING ORGANIZATION REPORT NUMBER. Enter all unique alphanumeric report numbers assigned by the performing organization, e.g. BRL-1234; AFWL-TR-85-4017-Vol-21-PT-2.

9. SPONSORING/MONITORING AGENCY NAME(S) AND ADDRESS(ES). Enter the name and address of the organization(s) financially responsible for and monitoring the work.

10. SPONSOR/MONITOR'S ACRONYM(S). Enter, if available, e.g. BRL, ARDEC, NADC.

11. SPONSOR/MONITOR'S REPORT NUMBER(S). Enter report number as assigned by the sponsoring/ monitoring agency, if available, e.g. BRL-TR-829; -215.

12. DISTRIBUTION/AVAILABILITY STATEMENT. Use agency-mandated availability statements to indicate the public availability or distribution limitations of the report. If additional limitations/ restrictions or special markings are indicated, follow agency authorization procedures, e.g. RD/FRD, PROPIN, ITAR, etc. Include copyright information.

13. SUPPLEMENTARY NOTES. Enter information not included elsewhere such as: prepared in cooperation with; translation of; report supersedes; old edition number, etc.

14. ABSTRACT. A brief (approximately 200 words) factual summary of the most significant information.

15. SUBJECT TERMS. Key words or phrases identifying major concepts in the report.

16. SECURITY CLASSIFICATION. Enter security classification in accordance with security classification regulations, e.g. U, C, S, etc. If this form contains classified information, stamp classification level on the top and bottom of this page.

17. LIMITATION OF ABSTRACT. This block must be completed to assign a distribution limitation to the abstract. Enter UU (Unclassified Unlimited) or SAR (Same as Report). An entry in this block is necessary if the abstract is to be limited.

Pulsed Microwave Plasma Instrumentation for Investigation of Plasma-Tuned Multiphase Combustion (DURIP)

Final Technical Report for work Executed Under AFOSR Grant FA9550-15-1-0195
Performance period: Sept. 2015-Sept. 2016

Submitted by

Dr. Travis Sippel, PI
515-294-3803 (phone)
515-294-3261 (fax)
tsippel@iastate.edu

Dr. James Michael, co-PI
515-294-0723 (phone)
515-294-3261 (fax)
jmichael@iastate.edu

Stuart J. Barkley, Ph.D. student
Keke Zhu, Ph.D. student

Iowa State University
Department of Mechanical Engineering
2025 Black Engineering
Ames, IA 50011

TABLE OF CONTENTS

LISTING OF FIGURES

LISTING OF TABLES

1. Executive Summary

This report describes the twelve-month Iowa State University effort to develop instrumentation for microwave enhancement of energetic materials, their flames, and to characterize microwave properties of energetics. Specifically, experimental facilities are developed to enable coupling of both continuous wave (CW, ~1 kW average power) microwave energy and pulsed, microsecond-duration (~0.5 to 2 μs duration, 10% duty cycle, 300 W average power) discharges of 2.45 GHz wavelength with composite solid propellants and their flames. Such instrumentation, in support of investigation of electromagnetic wave interaction with energetic materials and flames thereof is of interest due to the potential to perturb from steady state, an energetic material combustion wave through deposition of electromagnetic energy to either the propellant flame structure or to the propellant condensed phase, and the potential to develop microwave-sensitive energetic materials that may enable a number of effects within a burning energetic material such as microwave ignition, acceleration of burning rate, extinguishment, and re-ignition. *The effort to fabricate and validate this instrumentation was additionally supported, simultaneously, by AFOSR # FA9550-15-1-0481, "Interaction of Pulsed Microwave Plasma with Alkali Doped Propellant Combustion Flames," which describes in detail the mechanisms through which microwave radiation may be coupled to a propellant, its flame structure, and dynamic control techniques that can be enabled.* Specifically, the instrumentation developed in this effort comprises 1) an atmospheric pressure TE_{01} fundamental mode resonant microwave cavity with optically accessible propellant combustion flow through test section, 2) investigations using the cavity with both CW and pulsed microwave (MW) sources, and 3) measurement of propellant condensed phase dielectric properties at microwave frequencies for determination of condensed phase microwave power loss.

2. Background and Project Motivation

Strategies to control solid rocket propellant regression rate requires a robust throttling technique applicable to high performance propellant formulations. Currently, several methods to control and throttle either motors or subscale propellant strands exist, including chamber pressure control (e.g. pintle nozzles or rapid depressurization quench) [1], infrared laser irradiation of the burning surface to increase burning rates [2], development of inherently unstable combustion chamber geometries (producing either local pressure or velocity perturbations) [3], and electrically sensitive hydroxylammonium nitrate (HAN)-based formulations in which burning rate is controlled by a voltage potential [4]. However, these techniques are limited in that they either can only be used with low flame temperature (low specific impulse) propellants, result in low propulsion system mass fraction (pintle), are only capable of producing a single perturbation, or are formulation specific.

To gain control over a combustion process, combustion plasma enhancement has been demonstrated in electrothermal-chemical (ETC) launchers, in which solid gun propellant ignition flame spread, pressurization rate, and global propellant burning rate improvements were observed [5], [6]. With ETC enhancement, burning rate improvement of up to 35% is possible [7] and further enhancement is speculated to be possible with higher solid loading [8]. However, ETC launchers (e.g. capillary plasma generation) are capable only of single plasma injections or have limited volume (10's of centimeters in length) [9].

In consideration of a microwave- rather than ETC-generated plasma, the microwave transparency of many propellant ingredients [10], [11] may enable large volume plasma generation in complex grain shapes and microwave plasma seeding techniques are limited in number of plasma events by only energy availability. Unlike pintle throttling techniques, modification of a motor for microwave enhancement requires no moving parts and is simplified by utilization of the motor casing as an in-situ waveguide, requiring only the addition of an RF pressure window transition for magnetron interfacing. The use of microwave seeded plasmas within motors for control may also reduce aerodynamic loss (compared to pintle) and may enable throttling of higher performance propellant formulations (e.g. aluminized composites) that have flame temperatures too high to be easily controlled with pintle nozzles.

Pulsed microwave seeded-plasma generation is a multi-shot technique that has been used to gain control over combustion processes. This technique exploits low duty cycle, high power microwave pulses, for precise control over plasma growth. One strategy for pulsed microwave plasma generation involves operating in a subcritical regime, below the threshold for ionization in the ambient gas, where microwave energy deposition to the flame is facilitated through interaction of high field strengths produced from a ~100 kW pulsed source with weak electron populations produced from chemiionization radicals. This strategy allows for preferential coupling to regions of locally high ionization while avoiding parasitic gas breakdown and absorption at other locations[14]–[18]. Previously, this approach been demonstrated for both laser-generated ionization [14], [17] and in atmospheric pressure hydrocarbon flames [18]. Successful attempts at microwave supported plasma enhancement of premixed gas-phase flames [18] resulted in an increase in flame speed, a ~500 °C increase in flame temperature, and extension of lean flammability limits. The high field strengths able to be produced using pulsed techniques (order

10-100 kV/m) require only very low levels of ionization to rapidly establish plasma seeding and growth. However, seeding and growth are possible at much lower field strengths through non-equilibrium thermal ionization of a small amount of an easily ionizing dopant.

The use of a novel alkali metal doping technique for efficient, targeted low power (field strength) microwave energy deposition to the flame structure in order to seed the formation of a combustion-enhancing plasma has been demonstrated. With this technique, the propellant is doped with a small quantity of material containing easily ionizing atoms, such as alkali earth metals (e.g. sodium in form of sodium nitrate, $NaNO_3$). In doing so, microwave energy can be targeted to free electrons in a propellant flame, in order to produce the formation of plasma seeding (Fig. 1). With application to composite solid propellants, atmospheric pressure burning rate enhancement of ~21% with low amounts of dopant (~3-4 wt. %). Briefly, propellant containing dopant (e.g. sodium in the form of sodium nitrate, $NaNO_3$) is decomposes from thermal energy provide from combustion, producing Na^+ ion and electron in the flame. During microwave radiation, these ions and free electrons in the flame become energy deposit sites producing plasma kernels which grows throughout the flame. Plasma kernels form near combusting Al agglomerates due to high local flame temperatures. Including plasma combustion enhancement, two other rate enhancing mechanisms have been identified and are being studied: (1) condense phase heating in Maxwell-Wagner effect due to conductive particles in a non-conductive dielectric matrix(HTPB bind, AP) [19] and (2) combustion enhancement of burning Al agglomerates in the flame.

Regarding microwave absorption in the condensed phase (Fig. 1) of an energetic material, previous studies on S-band and X-band microwave absorption of metal filled polymer composites have measured the dielectric properties of micron size metal filled particulate composites, and show that the microwave loss tangent ($\tan(\delta)$) within metal particulates is strongly sensitive to particle size and composition [32]. Particle type and size has been shown to be important in determining metal particle energy absorption [31]. Metal particles are known to couple well with S- and X-band microwave radiation and can heat through eddy current mechanisms, with smaller metal particle sizes interacting more effectively with microwaves. While the interaction of high explosives (HMX, RDX, TNT) materials with microwaves has been investigated by measuring the dielectric properties via cavity perturbation of various formulations, [33] only very limited literature exist on the dielectric properties of different composite propellants ingredients (e.g. AP, HTPB) [10]. Further, no measured bulk properties of composite propellant formulations or models thereof currently exist in open literature. In order to advance microwave-seeded plasma throttling enhancement of composite solid propellant combustion, it is necessary to measure and be able to predict the microwave properties of the composite solid propellant condensed phase. An investigation is needed to explore condensed phase propellant properties in order to enable RF-thermal modeling and designing of resonant propellant strand cavities and motor configurations that efficiently utilize microwave energy to throttle combustion.

The complex permittivity of a material is given in real and imaginary components, where the real permittivity (ε') indicates the energy storage potential of the material and the imaginary component (ε'') indicates the dielectric loss of the medium. For a homogenous material, the dielectric properties are dependent on the material phase and lattices structure. When an electromagnetic field is applied to a homogenous medium, atoms, molecules, free charge and defects rearrange position during temperature- and frequency-dependent material relaxation. Such

properties are important to understanding (1) the thermal response of the condensed phase of an energetic during RF/microwave radiation exposure and (2) the effects of presence of a condensed phase (e.g. attenuation and impedance mismatch) on the field distribution within the non-condensed phase. In a propellant combustion application, while gas-phase absorption effects will occur, as a first step, one may first consider a non-participating gas medium. In doing so, to understand the effects of presence of a perfectly dielectric absorbing propellant condensed phase medium on field distribution and thermal response, the Helmholtz and heat equations (1), (2) are considered, where E is the electric field, ω is angular frequency, ρ is density, c is speed of sound, k is the thermal conductivity, T is temperature, and q_v" is volumetric heat generation. Furthermore, the volumetric heat generation due to permittivity loss within the RF/microwave field can be written as in equation (3). Condensed phase heating is important from a practical standpoint in order to develop microwave enhancement combustion models and to develop microwave power application regimes.

$$-\nabla^2 E = \omega^2 \varepsilon_0 (\varepsilon' - j\varepsilon'')E \tag{1}$$

$$\rho c \frac{\partial T}{\partial t} = k\nabla^2 + q_v'' \tag{2}$$

$$q_v'' = \omega\, \varepsilon''(E^2/2) \tag{3}$$

Though significant enhancement was observed from these experiments, the multimode, continuous wave cavity environment of these experiments frequently led to convective transport of plasma enhanced regions away from the burning surface, resulting in non-ideal deposition of energy to hot combustion products far from the burning surface. As such, significant burning rate enhancement beyond demonstrated improvements using continuous wave techniques, as well as improved combustion control is expected to be possible with pulsed microwave techniques. Pulsed microwave enhancement could take advantage of short seeding and plasma relaxation times to prevent parasitic energy deposition to features far from the burning surface, effectively optimizing heat feedback to the burning surface by "anchoring" plasma enhancement regions.

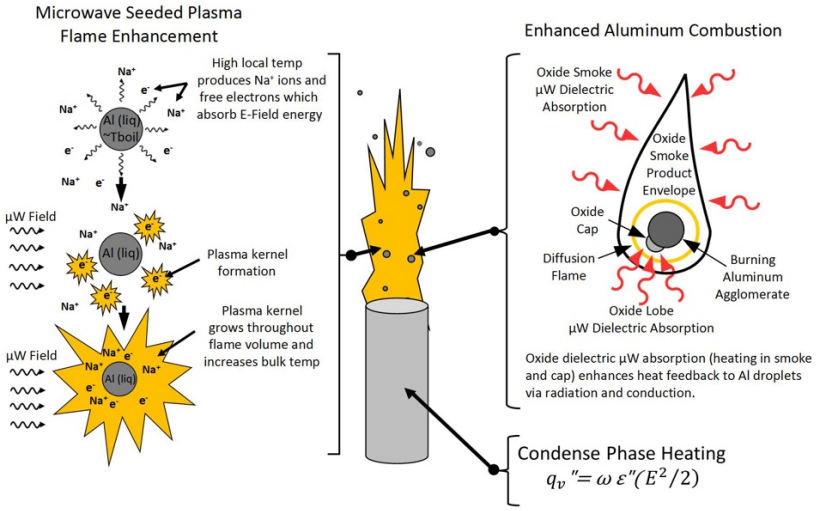

Fig. 1. *Illustration of possible mechanisms for burning rate enhancement. Plasma kernel seeding frequently occurs around Al particle flame structures due to high local flame temperatures and subsequently grows through the flame*

volume. Direct energy absorption (dielectric loss) to oxides (smoke and oxide cap) can occur. Condensed phase heating can also contribute to the burning rate enhancement.

3. Research Aims

The aims of this one-year effort are to (1) develop a resonant microwave combustion flow reactor for investigation of microwave interaction with doped and undoped energetic material flames (2) investigate the effects of high field strength, pulsed microwave discharges, as compared with CW microwave fields, with energetic materials and their flames, and (3) exploration of the effects of MW radiation with energetic materials and flames thereof.

4. Experimental Methods

4.1. Atmospheric Pressure Resonant Microwave Combustion Cavity (CW Experiments)

A single-mode, impedance-matched, resonant microwave cavity fitted with a flow through microwave applicator (Fig. 2a) was fabricated in order to explore effects of microwave energy interaction with composite solid propellant flames. Cavity energy is supplied by a circulator-protected 870 W, 2.46 GHz continuous wave (CW) magnetron (National 2M107-825) launched into a WR284 waveguide cavity and propagated in a TE_{10} resonant mode. The cavity is impedance matched to the load using a three-stub tuner, and calibrated, rectifying Schottky diodes (Pasternack PE8003) are used to monitor forward and reflected microwave power via a high-speed oscilloscope (Tektronix MSO 70404C). The microwave applicator is a choke-modified rectangular waveguide section containing two optical access ports in the E-plane and gas inflow/outflow choke ports in the H-plane (Gerling Applied Engineering). To prevent exposure of microwave components to corrosive propellant combustion exhaust, the applicator is modified by insertion of 19.81 mm thick press-fit polytetrafluoroethylene (PTFE) blocks on both sides of the applicator. The propellant and flame structure are positioned within the microwave applicator atop a PTFE stand and to improve flame observation, smoke is evacuated from the cavity by an air co-flow produced by light vacuum application to the top applicator choke. The cavity is terminated by a sliding short circuit, which is adjusted to generate a standing wave electric field antinode at the propellant/flame location, as shown in Fig. 2b. To compensate for presence of the PTFE blocks within the cavity, COMSOL Multiphysics 5.0 [25] was used to simulate the unloaded cavity and select the length of the sliding short circuit. To match cavity impedance to that of the propellant load, a half-length propellant strand (~1 cm) was placed in the cavity and the stub tuner was adjusted to minimize reflection. The quality factor (Q-factor) of the unloaded microwave resonant cavity was measured utilizing a vector network analyzer (VNA, Anritsu MS46322A Shockline) and was determined to be ~80.

Electric field strengths within the waveguide test section were estimated with analytical solutions of Maxwell's equations and a numerical solution of the exact cavity geometry. For the waveguide resonant cavity consisting of WR284 waveguide, the analytical solution of Maxwell's equations for a transverse electric field mode (TE_{101}) can be used to calculate field strength [26]. The root-mean-square (RMS) E-field strength is estimated as 91 kV/m at cavity test conditions within an adiabatic temperature, 3.5 wt. % $NaNO_3$-doped, aluminized propellant flame (1 kW magnetron output power, Q-factor of 80, 1 atm pressure, T_{ad}=3032 K). This E-field is cast as a reduced electric field by normalizing by the neutral gas number density, as estimated from the adiabatic flame temperature and pressure, giving an upper bound for E/N of 38 Td (10^{-21} V m^2).

This upper limit estimate of field strength is based upon measurements of an empty cavity. The cavity with a propellant strand partially inserted gives a similar Q factor. A lower bound (e.g. worst case) estimate of the E-field strength of the experiment can be made from consideration of the case where no energy is stored in the cavity. A numerical simulation (COMSOL Multiphysics) was conducted on the modified geometry in the microwave waveguide pass-through test section with an input port (TE_{10} mode, 1 kW of power) (Fig. 2c). PTFE blocks and gas inflow/outflow choke ports were included in this simulation in order to match the experimental setup. The RMS electric field strength in the cavity test location is estimated as ~38 kV/m (~16 Td at previously noted experimental conditions). Therefore, we estimate the RMS E-field strength of the microwave resonant cavity experiment is between 38-91 kV/m (~16-38 Td for the atmospheric pressure propellant flame environment). This bounded estimate is relevant to times during plasma kernel formation and early growth only, as the formation of a large plasma is expected to act as an energy sink and would effectively spoil the quality of the cavity resonator.

For combustion experiments, ~2 cm long propellant strands were positioned such that the burning surface was located at the top of the applicator and over the duration of an experiment (typically ~10 s duration), the burning surface would traverse the entire E-plane. Propellant strands were ignited by a one second duration, ~30 W CO_2 laser illumination. Immediately following CO_2 laser irradiation, the microwave field was modulated on and acquisition was started. Light diagnostics included direct emission observation via high speed video (Phantom ir300 with 50mm Nikon lens, 1 kHz) and high magnification backlit observation (Photron Fastcam SA-X2 with Infinity K2 microscope lens, 12.5 kHz frame rate, 0.293 μs exposure). Measurements of microwave-enhanced and unenhanced propellant burning rate were made from analysis of high speed video. High magnification backlit imaging was used to observe microwave field effects on the combustion of burning aluminum agglomerates within the propellant flame structure. Spectroscopic measurements (VIS-IR, OceanOptics USB4000, 5 Hz) were made of flame emission to estimate sodium temperature by a two-line emission technique. The two emission bands for Na at 589 and 818nm were collected simultaneously and filtered with two long-pass Schott glass filters (Thorlabs, FGL590 and FGL610). Light emission was imaged onto a 200 μm multimode fiber with a 50 mm diameter achromatic lens and coupled to the spectrometer. During combustion experiments, forward and reflected diode power measurements were used to monitor time-dependent microwave absorption of the propellant flame. As burning surface regression of a propellant strand causes insertion length of the propellant within the microwave applicator to change over the duration of a combustion experiment, the microwave absorption of the condensed phase (no flame) was measured as a function of propellant insertion length. These measurements were then compared with online absorption measurements taken from burning propellants to estimate the respective microwave absorption of the condensed phase and the flame structure over the duration of combustion experiments.

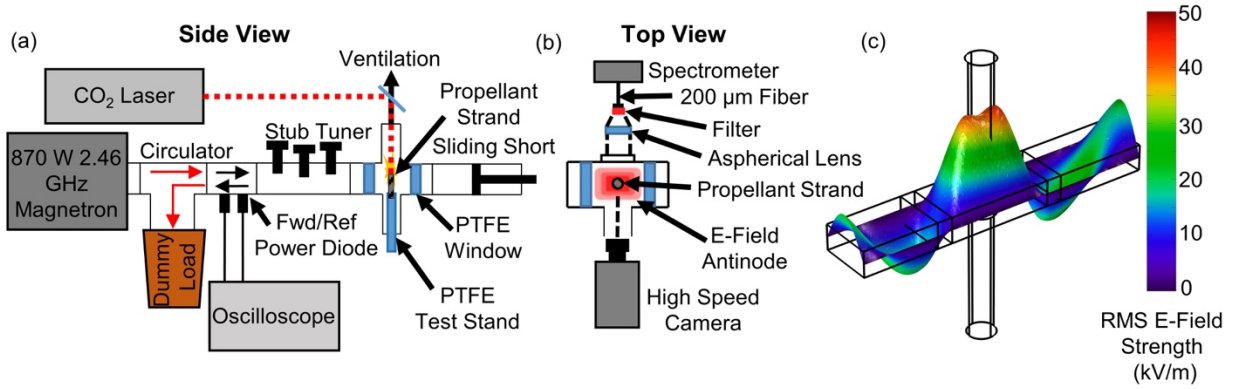

Fig. 2. *(a) Schematic of experimental setup of the microwave resonant cavity, which includes a circulator-protected magnetron launch, forward and reflected directional coupler with diodes, a three-stub tuner to match propellant load impedance, a flow-through propellant combustion microwave applicator, and a sliding short circuit. (b) The top view of the combustion applicator shows optical access on both sides, where a high-speed camera and spectrometer collected data on burning rate and combustion flame emission. (c) COMSOL 5.0 simulation of microwave applicator test section E-field distribution with no energy stored in the system (lower bound E-field strength). The RMS E-field strength within the propellant flame volume is ~38-91 kV/m.*

4.2. Pulsed Microwave Field Application

The aforementioned resonant microwave cavity was modified to interface with a Pulsed Systems 3.00 GHz, 30 kW peak power microwave generator with a New Japan Radio S-band magnetron (M1302A). Pulse duration and repetition rate were set to 2 μs and 500 Hz, respectively (0.001 duty cycle). This pulse duration and duty cycle were used, as they were observed to produce significant microwave coupling. Power was transmitted to the propellant via a circulator, power coupler, three stub tuner, applicator section, and a sliding short (Gerling) (Fig. 2). The source was protected with a dummy load at the circulator return. The cavity was initially tuned using a candle flame, then tuned to the final position with a propellant flame. Ignition was achieved by 450 nm, 1.5 W laser irradiation of the propellant burning surface. During combustion of propellant, the test section had a slight negative pressure applied to vent products from the test section. Teflon microwave windows were placed within the waveguide, isolating the combustion test section as shown in Fig. 2, to protect the short and stub tuner from the gaseous and condensed propellant combustion products. During microwave irradiation, forward and reverse power measurements were made using Schottky diodes (Pasternack PE8003) to determine time-resolved microwave energy absorption of the propellant flame and the condensed phase. Diode measurements were acquired using an oscilloscope (Tektronix MSO70404C) acquiring at 2.5 GS/s. Prior to use, diodes and the pulsed microwave source were calibrated by measurement of forward pulsed source average power using an Agilent E4418B average power meter. Diode response was then measured from the calibrated pulsed source. Typical diode voltages for experiments were between 500 and 300 mV, just below the linear response region of the diodes. The experimental data from the diode measurements was processed and converted into normalized absorptions using Eq. (4), where α is the normalized absorption, Fwd is the forward power, and Ref is reflected power. A Photron Fastcam SA-X2 with a Nikon 60 mm macro lens was used to capture high speed image sequences of the microwave pulse supported plasma enhancement of the propellant flame at 40,000 kHz and 10 μs exposure. A digital pulse delay generator (Berkeley Nucleonics) was used to trigger the microwave generator and high-speed camera to acquire video data of multiple, distinct plasma events during a combustion experiment.

$$\alpha = \frac{Fwd-Ref}{Fwd} \quad (4)$$

Propellant formulations investigated using the pulsed microwave source are shown in Table 1, and are fabricated using the methods described in Section 4.5.

Table1. *Propellant formulations used for pulsed microwave field application experiments.*

	Propellant Composition (wt. %)				
Formulation Name	**$NaNO_3$ (< 75 µm)**	**cAP (200 µm)**	**fAP (< 90 µm)**	**Al (30 µm)**	**HTPB**
Al-AP-$NaNO_3$ 3.5%	3.5	56.4	14.1	14.5	11.5
Al-AP-$NaNO_3$ 1.0%	1.0	57.8	14.4	14.9	11.9
Al-AP-$NaNO_3$ 0.1%	0.1	58.3	14.6	15.0	12.0
Al-AP	0.0	58.4	14.6	15.0	12.0
AP	0.0	70.4	17.6	0.0	12.0

4.3. Additional Diagnostics: Sodium Two-line Temperature Measurement

Utilizing the spectra collected during non-microwave- and microwave-enhanced propellant combustion experiments, the electronic temperature of sodium was estimated based on a pair of emission lines at 589 and 818 nm. Emission at 589 and 818 nm (3p-3s and 3d-3p transitions, respectively) are a result of the electronic excitation of Na by inelastic collisions with atomic and molecular species as well as free electrons. For the applied RMS electric field strength of ~30-90 kV/m, a typical free electron temperature in the microwave plasma might be ~0.5 to 1 eV [27]. The temperature measurement resulting from comparison of the emission strengths of these two lines should lie between the translation and electron temperature for the system. For spontaneous emission from the two transitions considered, the total emission intensity can be written as the product of the spontaneous emission rate, the degeneracy, and the population fraction in the upper state for the transition. Assuming local thermal equilibrium (LTE) [28,29], a Boltzmann distribution giving the population fraction can be used to infer the electronic temperature of sodium T_{Na} by using the signal intensity ratio for spontaneous emission from two transitions corresponding to transitions from state j to i and state n to m. The ratio between signals is given by

$$\frac{S_{n,m}}{S_{j,i}} = \frac{\eta(\lambda_{n,m})}{\eta(\lambda_{j,i})}\frac{QE(\lambda_{n,m})}{QE(\lambda_{j,i})}\frac{\sum_n A_{m,n} g_m e^{-E_m/k_B T_{Na}}}{\sum_j A_{j,i} g_j e^{-E_j/k_B T_{Na}}}, \quad (5)$$

where g_j is the degeneracy of state j, $A_{j,i}$ is the spontaneous emission rate from state j, E_j is the energy of the upper state, and k_B is the Boltzmann constant. Constant factors η and QE represent the optical collection efficiency and quantum efficiency, respectively, which are constant for each line transition j,i or n,m tied to the respective transition wavelength $\lambda_{j,i}$. The spontaneous emission coefficients and degeneracies are taken for sodium [30,31] for the given transitions. By writing the

ratio of emission bands, factors including the emission collection efficiency, filter transmission functions, and sensor quantum efficiency can be neglected. This was particularly important due to the relative differences in emission intensity between the 589 nm and 818 nm features. As described in Section 2.3, the 589 nm emission was attenuated via filtering to allow both features to fit well within the dynamic range of the spectrometer sensor. Spectra were collected during the entire duration of the propellant burn and the integrated emission over each band was taken as the total band intensity. The broadband contribution from blackbody emission due to condensed phase products was baseline subtracted and the intensity of both 589 nm and 818 nm bands were calculated by integrating emission from the two peaks.

Sodium two-line temperature experiments were conducted on burning propellant strands exposed to a 200 ms duration microwave pulse at 1 Hz during the 10 s duration propellant combustion event. The intensity ratios were calculated for each acquisition frame, and were used to determine an average intensity ratio for microwave-irradiated and unirradiated flame conditions. The average signal ratio for the unirradiated case was used to establish a baseline emission peak ratio associated with an estimated temperature given by the adiabatic flame temperature (3032 K). When the microwave was then switched on, the change in the ratio was used to estimate a new temperature by taking the factors η, QE, A, and g, as constant between the two cases. This inferred temperature represents the change in distribution of the states of electronic sodium and we assume these states are in LTE to infer a temperature.

4.4. Equilibrium Chemical and MW Energy Absorption Calculations

Equilibrium calculations conducted with varying propellant reactant composition and sodium dopant levels (Fig. 3a**)** indicate that Na ion concentration and free electron concentration are optimized for formulations containing ~22 wt. % aluminum, where the highest adiabatic propellant flame temperatures occur and are expected to produce the greatest level of sodium thermal ionization. However, Na ion concentrations are maximized at lower $NaNO_3$ loadings as compared to free electron concentrations. Holding aluminum content constant at 15 wt. %, the overall effect of dopant addition is a reduction in flame temperature and a subsequent decrease in specific impulse (I_{sp}), determined for typical motor pressures of 1000 psi. Replacement of 16 wt. % AP with $NaNO_3$ in a 15 wt. % aluminized propellant (Table 1) is found to reduce I_{sp} by 11 s from 262 to 251 s. However, at lower dopant levels, replacement of 3.5 wt. % of AP with $NaNO_3$ reduces I_{sp} by only 2 s. While higher equilibrium free electron concentrations are accessible with $NaNO_3$ dopant addition beyond 16 wt. %, the associated decrease in I_{SP} performance is significant. However, low dopant additions present an advantageous opportunity to increase free electron populations within propellant flames at the cost of only a small specific impulse reduction.

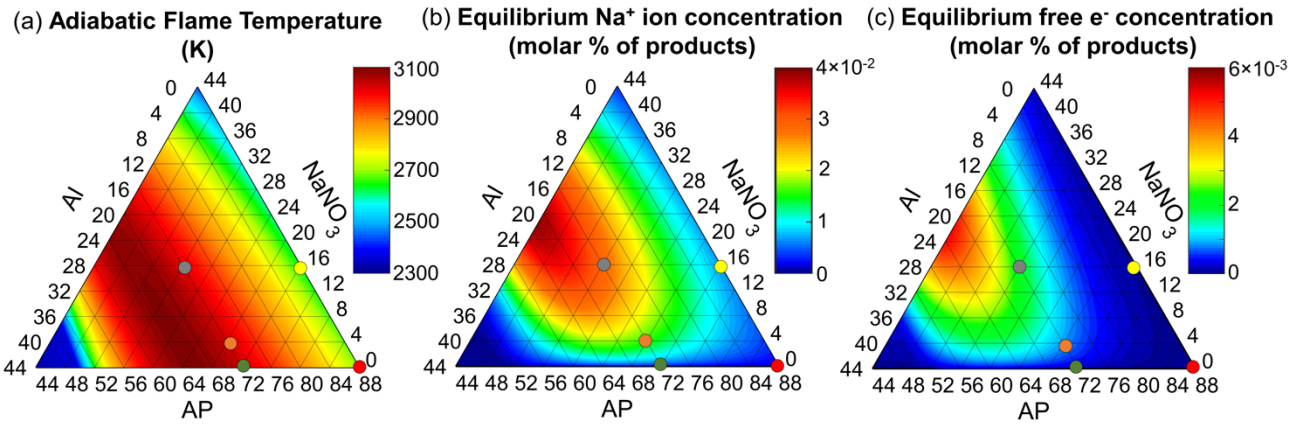

Fig. 3. *Equilibrium calculation of adiabatic flame temperature (a), Na ion concentration (mol. % of chamber products) as a function of propellant formulation (b) and calculation of free electron concentration (mol. % of chamber products) as a function of propellant formulation (c). Calculations are conducted at 1 atm pressure. Each corresponding color point indicates a corresponding formulation experimentally investigated in Fig. 4.*

Trend lines in Fig. 4 confirm that vibrational excitation is the dominant energy absorption pathway for all but the most extreme reduced field conditions. More significantly, the trend lines for ionization suggest that a mole fraction of only 0.284% atomic sodium is capable of absorbing significantly more field energy for the purposes of ionization than the rest of the gas mixture combined. Sodium excitation and ionization is expected to be more favorable than other species due to the low electronic and ionization energies, and over the range of 40-80 Td, the absorption of field energy into electronic excitation is dominated by inelastic electron collisions with atomic sodium. This significant increase in ionization is observed in experiments, to be discussed in the experimental results to follow. Additional simulations neglecting sodium confirmed that the energy absorption rates for the remainder of the gas mixture were not significantly modified by the presence of sodium.

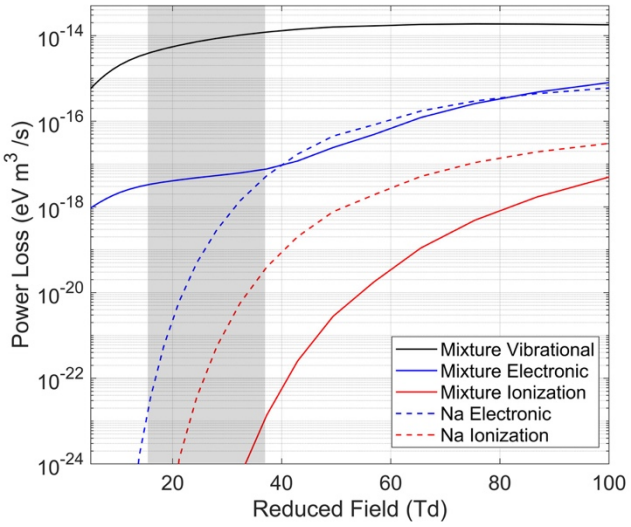

Fig. 4. *Electron power loss rates, normalized by number density, for each of the pathway groupings over a range of reduced field strengths. RMS field strength at each reduced field value is reported using the temperature and pressure conditions described in Table 1 to obtain ideal gas number density. The grey region indicates the estimated range of reduced fields observed in the following experiments.*

4.5. Propellant Manufacture

Five different composite propellant formulations were manufactured varying the amount of aluminum, AP, and $NaNO_3$ dopant. The propellant formulations, shown in Table 2, consisted of aluminum (~35 μm, Valimet-H30), AP (200/90 μm, 80/20 coarse/fine wt. %, Firefox Chemicals), $NaNO_3$ (Firefox Chemicals), and an HTPB binder system. Prior to propellant fabrication, $NaNO_3$ was milled and sieved to achieve particle sizes of < 75 μm and propellant solids were dried under roughing vacuum at 50 ºC for one day. The binder system consisted of R45 monomer (Firefox Chemicals), isodecyl pelargonate (IDP, Firefox Chemicals) plasticizer, HX-878 (tepanol, Firefox Chemicals) bonding agent, and IPDI isocyante curative (Firefox Chemicals). The propellant formulations were mixed for three hours in a dual planetary mixer and deaerated at room temperature and under roughing vacuum for 30 minutes. Strands were cast into 6-mm-diameter cylinders using polyethylene molds and allowed to cure for seven days at 60 °C in an explosion proof oven. After curing, propellant strands were cut to ~2 cm lengths. Measured densities of cured propellants were greater than 95% of theoretical maximum density (TMD). For combustion experiments, the surfaces of propellant strands were inhibited to prevent flame spread down the sides of the burning strands.

Table 2. *Solid propellant formulations with corresponding equilibrium predictions of electron mole fraction ($[e^-]$), equilibrium specific impulse (I_{SP}), adiabatic flame temperature ($T_{flame,ad}$), and experimentally observed atmospheric pressure propellant burning rate (r_b) with and without microwave enhancement. All formulations contain ~12 wt. % HTPB binder. Specific impulse (I_{SP}) is computed with a chamber pressure of 6.89 MPa with an expansion ratio of 68. All other data are computed/measured at 1 atm pressure. Burning rates (r_b) are reported as the average and standard deviation of three experiments.*

Formulation, balance HTPB	**$NaNO_3$ Dopant (wt. %)**	**$[e^-]$ (mol. frac)**	**I_{SP} (s)**	**$T_{flame, ad}$ (1 atm), (K)**	**r_b w/o MW (mm/s)**	**r_b w/ MW (mm/s)**	**r_b Enhancement**
AP (88 wt. %)	0%	1.11×10^{-10}	251	2713	1.17±0.008	1.20±0.031	3.0%
AP/$NaNO_3$ (72/16 wt. %)	16%	8.65×10^{-7}	240	2664	0.624±0.028	0.753±0.047	20.7%
AP/Al (73/15 wt. %)	0%	2.13×10^{-7}	262	3031	1.07±0.039	1.17±0.027	10.1%
AP/Al/$NaNO_3$ (70.4/14.5/3.5 wt. %)	3.5%	7.54×10^{-6}	260	3032	0.988±0.017	1.26±0.015	27.5%
AP/Al/$NaNO_3$ (57/15/16 wt. %)	16%	2.03×10^{-5}	251	3011	0.522±0.012	0.847±0.006	62.3%

4.6. Dielectric Property Measurement

Measurements of the dielectric properties of AP composite solid propellants were conducted using a vector network analyzer configured in a transmission mode measurement. The propellants used in this study were produced in batches of 800 g and formulations for propellants are shown in Table 3. Propellants utilized a HTPB binder system consisting of R45 monomer (Firefox Chemical), isodecyl pelargonate (IDP, Firefox Chemical) plasticizer, desmodour curative,

and HX-878 (tepanol) bonding agent (RCS Rocket Motor Parts). Prior to mixing, ingredients were dried in an oven at 60 °C. Propellants were mixed for three hours in a six-quart dual planetary mixer. Propellant was deaerated at room temperature for 30 minutes at vacuum pressure and was cast using 3D printed rectangular casting molds and molds were placed in an explosion proof oven at 60 °C (140 °F) for a week to cure. The dimension of cured S-band propellant blocks was 7.264 x 3.450 cm (2.860 x 1.360 in) with length of 2.912 cm (1.1465 in). After curing, the propellant was finished to appropriate dimensions to be installed inside a WR-284 waveguide for dielectric measurement (Fig. 5).

Table 3. *Propellant formulations used in this study to investigate effects of $NaNO_3$, AP, and Al particle size.*

	Propellant Composition (wt. %)				
Formulation	**$NaNO_3$ (< 5 μm)**	**cAP (200 μm)**	**fAP (< 90 μm)**	**Al (30 μm)**	**HTPB**
f$NaNO_3$, bimodal AP	3.5	49.2	12.3	17	14
cAP, fine $NaNO_3$	3.5	61.5	---	17	14

Calibration and measurement procedures were followed based on the National Institute Standard and Technology (NIST) standard for transmission line dielectric properties measurement[15]. Prior to dielectric property measurement, the VNA was calibrated with WR-284 sliding short and waveguide section via the short-short-short-thru (SSST) method to establish the reference planes. Composite propellant test articles were placed into WR-284 waveguide sample holder. An Anritsu Shockline MS46322A vector network analyzer was used to measure S parameters (S_{11} and S_{21}) at 0.002 GHz intervals from 2.30 GHz to 2.65 GHz (Fig. 5). Propellant articles are assumed to be perfectly dielectric, with real permittivity (μ') of unity and imaginary permittivity (μ") of zero. This is because the propellant under test only contains AP, $NaNO_3$, Al, and HTPB, all nonmagnetic material. From these measurements the real and imaginary parts of the permittivity, loss tangent and conductivity are obtain utilizing the Nicholson-Ross-Weir (NRW) model [34]. The NRW method is commonly used to measure dielectric properties of low-loss materials over broadband frequency ranges [34]. Dielectric properties were additionally determined from accurately machined samples of Teflon and compared to literature values to verify both dielectric measurement techniques, and instrumentation calibration.

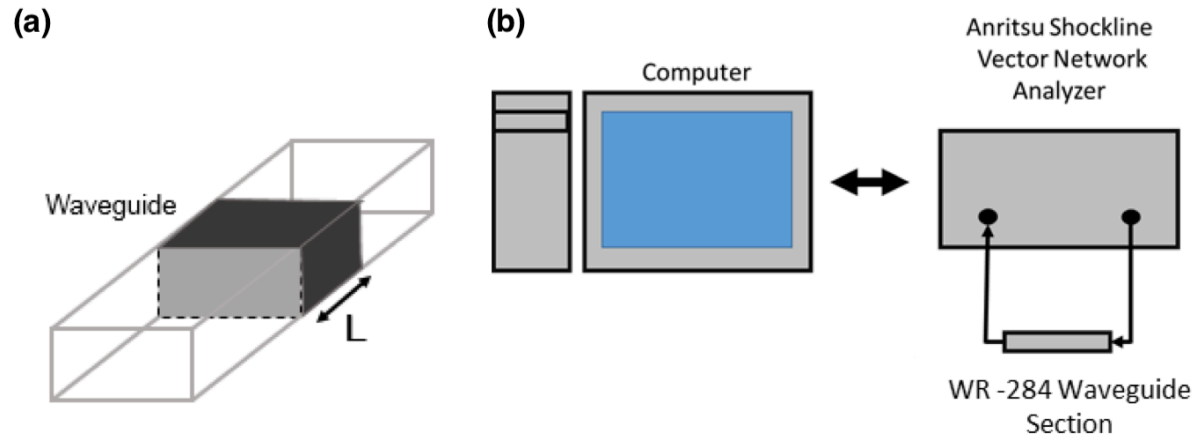

Fig. 5. *(a) Schematic of propellant test article in waveguide transmission measurement. Propellant test articles are 2.912 cm long (~λ/4 at ~2.7 GHz). (b) Experimental setups for measuring dielectric properties using the cavity perturbation technique with a vector network analyzer.*

5. Results

5.1. CW and Quasi-CW Microwave Effects on Flame Structure and Plasma Formation

Experiments were conducted for the range of formulations presented in Table 2. For these experiments, with estimated RMS electric field strength of ~38-91 kV/m, visible light emission was significantly enhanced during microwave application for all propellant formulations. In Fig. 6, still image sequences are shown of each propellant formulation burning both with and without microwave field application. For propellants without microwave enhancement (Fig. 6, left), the structures and emission intensities of flames from all propellant formulations appear uniform over the three-millisecond duration of the image sequences. Under microwave application (Fig. 6, right, and in supplementary video), flame emission intensity increases by ~4-13 times for all the propellant formulations. In comparing image sequences of microwave enhanced flames, the advantageous effects of dopant addition in promoting ionization and electronic state populations and enhancing overall microwave coupling are demonstrated.

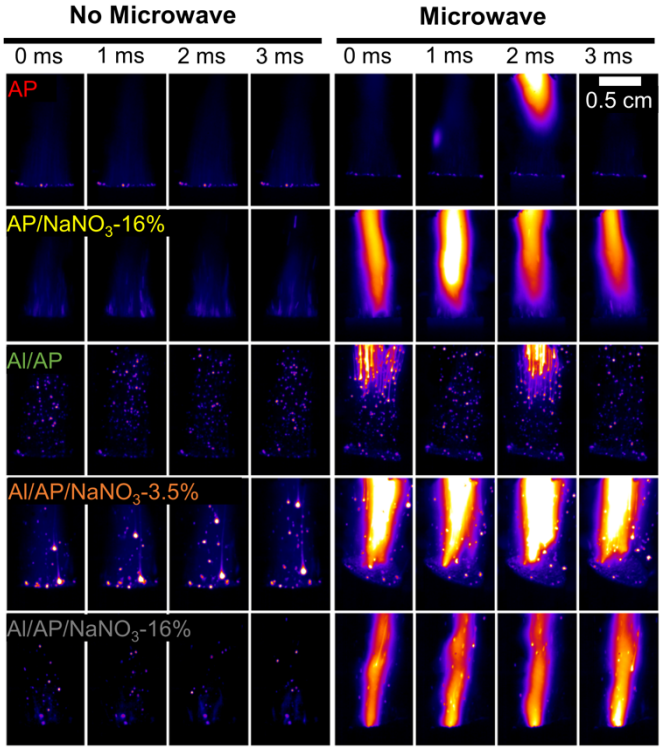

Fig. 6. *Still frame image sequences of the combustion emission of all formulations without (left) and with (right) microwave field application. Frames are shown with an inter-frame spacing of 1 ms. False coloring is used to indicate emission intensity. Camera exposure and aperture settings are the same for each formulation with and without microwave.*

Propellants without $NaNO_3$ dopant exhibit periodic emission enhancement. Energy deposition to these propellant flames suggests that even without a dopant, the flame temperatures are high enough, local electron populations are high enough, and densities are low enough to allow the rapid ionization of products and the formation of localized plasmas. The periodic emission seen in AP and Al/AP formulations without sodium dopant addition suggests the local electric field strength is only sufficient to sustain a plasma for short durations. One possible and significant source of electrons within undoped, unaluminized flames is from impurities in the propellant ingredients. Emission spectra (not shown) from microwave irradiated, undoped, unaluminized AP composite propellant flames contain trace impurities from calcium, potassium and, sodium atomic species and CaCl molecular species from the combination of the impurities with flame species [32]. Enhanced flame regions in undoped propellants are also not anchored with respect to the burning surface and can be seen translating away from the burning surface with the product flow. Finally, the periodic nature of these emission features suggests that other effects like field-induced polarization or local field enhancement due to local structures such as aluminum agglomerates may be important.

In comparing emission image sequences of undoped AP and Al/AP propellants, there are several distinct differences in microwave coupling regions which occur with the addition of aluminum to the propellant formulation. Within unaluminized AP propellants, kernel formation and growth are observed to occur within the propellant gas phase as shown by the diffuse structure of the luminous region during microwave field application. Within aluminized AP composite

propellants, significant emission enhancement can be observed from long vertical structures which are subsequently discussed in Section 3.3. The unique emission enhancement structure of aluminized propellants that results from microwave irradiation is suggestive of either ionization of atomic aluminum (5.99 eV ionization energy) or aluminum diffusion flame structures via another mechanism. Addition of $NaNO_3$ dopant to microwave irradiated is found to stabilize emission enhancement by anchoring enhanced regions close to the propellant burning surface. Enhanced near-burning surface anchoring was observed to be improved in propellants with increased $NaNO_3$ dopant concentration and/or from aluminized formulations. The most effective anchoring was observed in 15 wt. % aluminized propellants containing 16 wt. % $NaNO_3$ dopant, which have the highest equilibrium-predicted free electron population (Table 1) of all experimentally investigated formulations.

The Na spontaneous emission ratio was measured for the aluminized, 3.5 wt. % $NaNO_3$-doped propellant flame with and without microwave enhancement. From the emission ratio, the sodium temperature difference was calculated from the 818nm/589nm ratio, as previously described. Briefly, the mean of the ratio without microwave application was assigned a temperature corresponding to the adiabatic flame temperature calculation. To determine a temperature increase, the baseline ratio was calculated for the situation with no microwave application. The emission ratio during the application of the electric field was then measured, as shown in Fig. 7. The measured 818/589 nm ratio of a propellant flame is approximately 4 times higher as a result of microwave irradiation, indicating an increase of sodium electronic temperature of ~1000 K. In addition, the absolute emission intensity increased by a factor of ~4 for the 589 nm emission and ~16 for the 818 nm emission. The increase in the relative rate of emission from these states suggests both an increase in temperature and a potential increase in the processes resulting in population of the excited states of atomic sodium. These processes likely consist of inelastic collisions of sodium with excited atomic and molecular species as well as inelastic collisions with electrons. The increase in equilibrium-predicted electron population (without microwave irradiation) and the microwave-induced sodium temperature enhancement suggest the ability to form of a sodium plasma and indicates the important role of an alkali dopant such as sodium in lowering the threshold for microwave absorption to the propellant flame.

Collectively, these results suggest that electron populations within both aluminized and unaluminized composite solid propellant flames, regardless of whether a dopant is used, are high enough to couple with and allow energy deposition from a ~38-91 kV/m, 2.46 GHz E-field, and that energy deposition results in emission enhancement. While emission enhancement from undoped propellants appears periodic and unanchored, addition of either or both sodium nitrate dopant or aluminum to a propellant more effectively anchors emission-enhanced regions near the propellant burning surface. Application of a microwave field to a sodium-doped propellant flame results in significant increases in sodium temperature and sodium emission intensities. Both of these observations suggest that microwave irradiation results in large increases in free-electron populations and an increase in excitation of electronic states of sodium, which occur through inelastic collision with electrons and excited neutrals. Although absolute electron number density is not estimated, these results are consistent with the formation of a low density plasma controlled by the application of the microwave field.

Plasma enhancement has been shown to play an important role in other reacting systems, where the processes can be classified as mainly thermal (where populations are in LTE) and non-thermal,

where certain species may be far from equilibrium and may results in the activation of additional important kinetic pathways [33]. These pathways may well be important for the propellant microwave-enhancement, but are not directly observed on the timescales in this experiment. Ultimately, the burning rate enhancement is largely due to thermal feedback from the various energy deposition mechanisms to the propellant burning surface. However, the individual processes resulting in thermal energy transfer may be rate-limited by processes which may deviate from thermal equilibrium and include the production of significant radical populations.

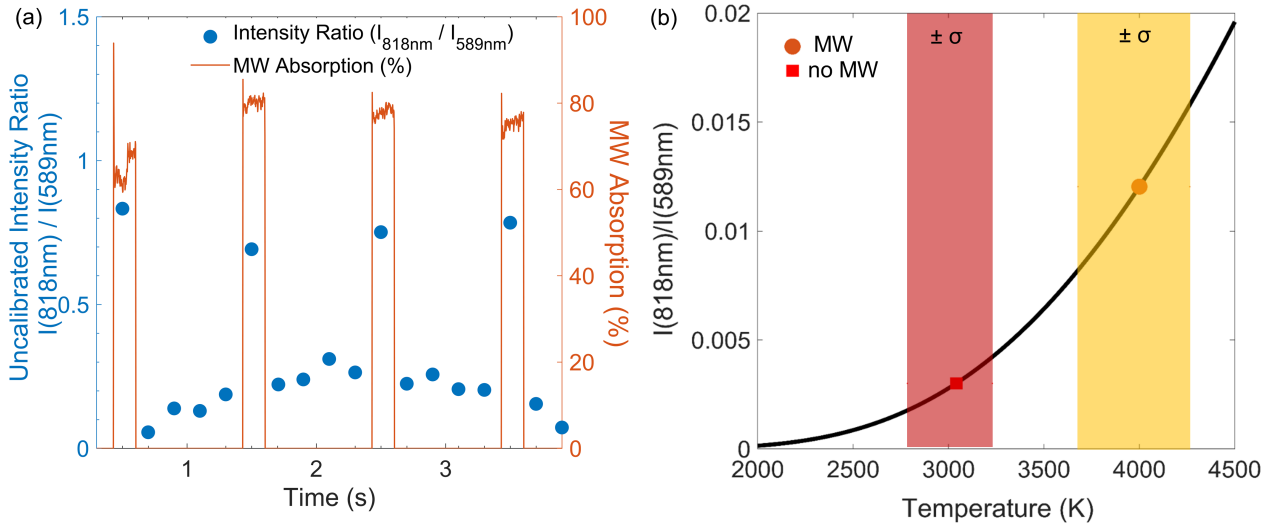

Fig. 7. *(a) Time history of line intensity ratio shown with the microwave absorption during a propellant burn with a 20% duty cycle modulated microwave field. (b) Average inferred sodium electronic temperature of aluminized, doped composite propellant (Al/AP/$NaNO_3$-3.5%) with and without microwave enhancement. Banded temperature regions indicate temperature ranges corresponding to +/- one standard deviation of measured sodium band emission intensity ratios for three propellant strand combustion experiment.*

5.2. Oxide Thermal Runaway Dielectric Absorption

From image sequences of microwave-enhanced propellant combustion (Fig. 8), energy deposition to aluminized propellant flames differs from unaluminized propellants significantly. In the aluminized AP propellant without dopant (Al/AP/HTPB), long emission enhanced features are observed. The typical aluminum agglomerate flame structure consists of a molten aluminum droplet/agglomerate, an attached lobe of aluminum oxide, a diffusion flame, and a condensed aluminum oxide smoke trail. High magnification imaging of the aluminum diffusion flame of an undoped propellant flame (Fig. 8) show that with field application, emission enhancement is observed in both the aluminum oxide condensed smoke and the aluminum oxide lobe attached to the burning aluminum agglomerate. Field application results in growth of the aluminum diffusion flame envelope in small aluminum agglomerates (~100 µm diameter and smaller), indicating faster liquid aluminum volatilization rates due to increased heat transfer to the aluminum through conduction (contact with the oxide lobe) and radiation (feedback from the oxide smoke envelope).

The image series in Fig. 8 shows increases luminosity from the aluminum oxide as a result of energy absorption. This graybody luminosity suggests significant increases in the aluminum oxide condensed phase product temperature and is hypothesized to result from strong dielectric energy

loss to the aluminum oxides. While the microwave-frequency dielectric loss tangent (tan δ) of aluminum oxide at room temperature is low (tan δ = 0.0003), at elevated temperature, dielectric loss increases exponentially due to electron promotion to valence shells. At an elevated temperature of 1500 K, the loss tangent of aluminum oxide is 300 times higher than at room temperature [34,35]. In an aluminized propellant combustion environment, where the surface of an aluminum agglomerate is at the aluminum boiling temperature (~2740 K, 1 atm) and aluminum diffusion flame temperatures are in excess of this temperature, microwave energy deposition to oxide products is expected to be even more efficient. The efficient deposition of microwave energy to aluminum oxide in a thermal runaway condition is similar to behavior demonstrated by others in several oxides [34,35]. As burning aluminum particles are convected away from the propellant burning surface, microwave energy deposition is localized in the hot aluminum oxide products and this process continues until the hot products convect out of the microwave cavity.

Within a composite solid propellant, the ability to enhance the temperature of the high emissivity, high specific surface area oxide product smoke of burning metals is of high utility, as radiation heating of a propellant burning surface is significant. The maximum oxide smoke temperature that can be achieved through microwave irradiation enhancement is limited thermodynamically by the oxide boiling temperature (3250 K, Al_2O_3, 1 atm). Thermodynamic scaling of these limiting conditions to a 2.03 MPa rocket motor environment with 900 K propellant burning surface temperature [36] and ~5000 K oxide volatilization temperature shows the energy envelope for sensible enthalpy enhancement of aluminum oxide is large. The nanoscale oxide smoke from aluminum diffusion flames within composite solid propellants are high flux emitters which re-radiate energy to the propellant burning surface and may provide significant, microwave-controlled enhancement to the propellant burning rate.

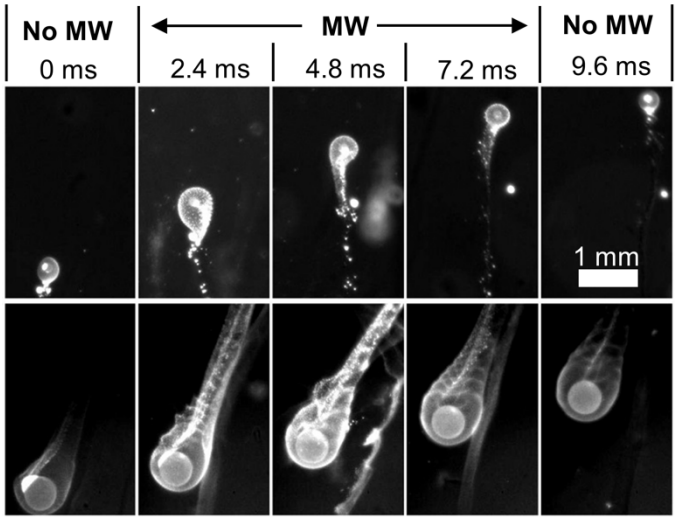

Fig. 8. *Two high magnification image sequences of aluminum agglomerate combustion near the burning surface of an Al/AP/$NaNO_3$-3.5% propellant with microwave modulation at 60 Hz. Increased emission intensity of the oxide smoke and oxide cap features indicate increased oxide temperatures due to dielectric absorption at high temperature.*

5.3. Microwave Energy Partitioning and Burning Rate Enhancement

The two previously described mechanisms (plasma formation and energy deposition to the gas phase, and dielectric loss to aluminum oxides) are expected to result in enhancement of composite solid propellant burning rate through improved heat feedback to the burning surface. In addition,

it is expected that some microwave energy may be deposited directly to the condensed phase of the composite solid propellant through both dielectric loss and for aluminized propellants, Maxwell-Wagner losses [37]. The total amount of incident microwave irradiation absorbed by both the propellant flame and condensed phase is apparent from comparing both forward and reflected power measurements over the duration of a propellant combustion experiment (Fig. 9(a,b)). Energy absorption remains high over the duration of the experiment (~60-90% absorption) but decreases as propellant combustion progresses, which is due to either cavity detuning or reduced condensed phase loss (Fig. 9(a)).

In order to quantify the partitioning of microwave energy deposition to either the gas phase flame or directly to the propellant condensed phase, measurements of the condensed phase absorption of Al-AP-$NaNO_3$-3.5 wt.% propellant were taken as a function of strand height within the microwave applicator cavity. These were compared to online absorption measurements of the same propellant burning within the cavity (Fig. 9(b)). During experiments, however, it was observed that for some formulations, flame spread occurred down the sides of latex-coated propellant strands, resulting in unplanar burning surfaces and artificially enhanced burning rates. Flame spread is likely due to either/both dielectric absorption of the latex inhibitor or plasma erosion of the surface. To prevent flame spread, propellant strands were burned within the 0.38 mm thick polyethylene tubes in which they were cast. The complex permittivity of polyethylene is relatively low (0.0005 at 1 GHz) and thermal loss to the polyethylene tube is low. As a result, there is only ~5% difference in burning rates between latex-coated (uninhibited) and polyethylene coated (inhibited) propellant combustion rates (Fig. 9b).

Considering energy partitioning to the flame or condensed phase (Fig. 9b), at the beginning of propellant strand burn experiments (strand height ~2 cm), absorption is high and is observed to decrease as the burning surface regresses. The absorption of the condensed phase remains high (~60%) from the beginning of the burn until strand height has regressed to ~1 cm and then decreases. A local absorption maxima of all burning propellant strands (flame present) were observed at a height of ~1 cm, which could be due to the shift in the cavity resonance during the burn, as the cavity was optimized for maximum quality using a half-height propellant strand. In comparing absorption of both the condensed phase and propellant with flame, roughly 20-25% of the incident microwave energy is deposited to the propellant flame structure and 40 to 60% is deposited to the condensed phase, while the remainder is reflected.

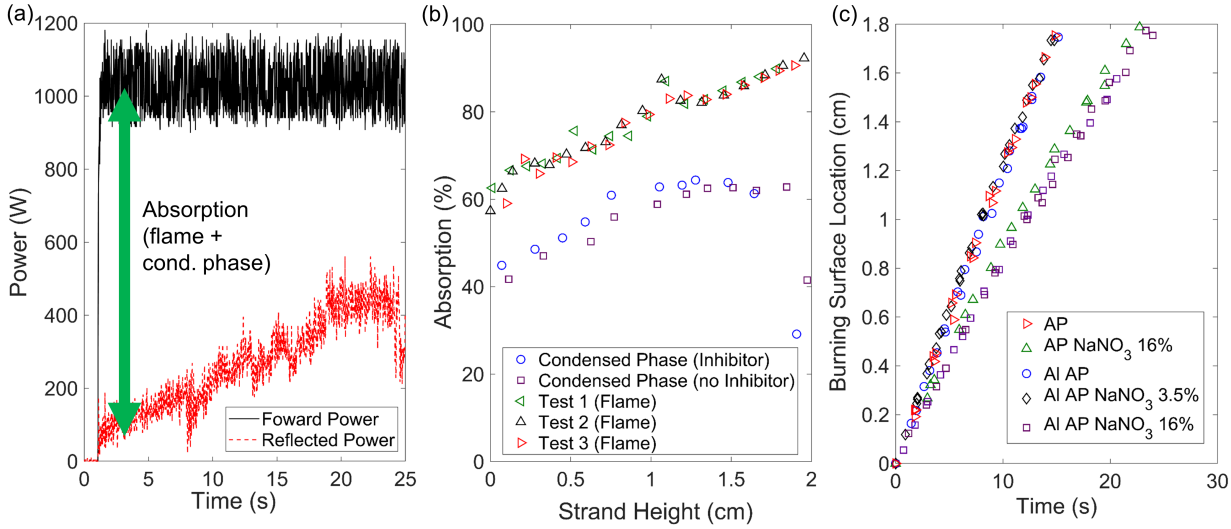

Fig. 9. *(a) Typical forward and reflected microwave power measurements taken during Al-AP-$NaNO_3$ combustion. (b) Typical microwave absorption measurements from three experiments conducted with an Al-AP-$NaNO_3$ 3.5 wt.% propellant as a function of propellant strand height within the cavity for both propellant condensed phase (no flame, with and without polyethylene inhibitor tube) and burning propellant (flame and condense phase present in microwave cavity). The propellant height was measured with respect to the bottom of the optical viewing window. (c) Typical measurements of burning surface location as a function of time for all formulations under microwave field application.*

The burning rates of composite solid propellant formulations studied in this effort were measured both without and with microwave irradiation through direct measurement of the regression surface location in time (Fig. 9(c)). In measurement of burning surface location with time, no acceleration of burning rate in time is observed in the formulations, which suggests microwave absorption directly by the condensed phase is not primarily responsible for burning rate enhancement. Average burning rates of propellants both with and without microwave irradiation are shown in Table 2 and in the supplemental video. The microwave burning rate enhancement of undoped, unaluminized propellant was 3%, and addition of 16 wt. % dopant increased the percent microwave burning rate enhancement to 20.7%. Aluminized propellants without dopant exhibited a 10.4% microwave burning rate enhancement as a result of microwave irradiation. Addition of 3.5 wt.% dopant to the aluminized propellant increases microwave burning rate enhancement to 27.4%, and further addition of dopant (16 wt.%) results in a 62.3% burning rate enhancement.

In considering the percentage burning rate enhancement observed with all propellants, we observe that the degree of burning rate enhancement possible under conditions of the experiments is increased by both addition of sodium nitrate dopant and addition of aluminum to the propellant formulation. These two findings are supportive of the proposed microwave energy deposition mechanisms, as (1) sodium nitrate addition increases the equilibrium flame free electron pool, enabling more efficient plasma support within the flame and nearer to the burning surface, and (2) energy deposition to aluminum oxide smoke flame features can enhance burning rate directly through enhanced thermal irradiation of the burning surface or indirectly through aluminum agglomerate burning rate enhancement.

5.4. Microsecond-Duration Pulsed Microwave Interaction with Composite Solid Propellant Flames

5.4.1. Pulsed Microwave Energy Absorption

Forward and reflected power measurements taken during the pulsed application of a 2 μs duration application of a 30 kW, 3.0 GHz microwave pulse indicate significant microwave absorption of the flame occurs. For all propellant formulations, absorptions and coupling of the propellant flame is observed. In each of the propellant formulations, propellants with $NaNO_3$ absorbed more microwave energy during the propellant burn than compared with the non-doped aluminized AP composite propellant and AP composite propellant (Fig. 10). This is expected to be a result of sodium thermal ionization and subsequent free electron absorption. Within doped propellants, short duration excursions of lower absorption are observed, which may be a result of microwave reflection resulting from charge shielding effects in highly ionized plasmas. These effects appear slightly more prevalent in propellants containing higher $NaNO_3$ dopant levels of 3.5 and 1.0 wt.%.

Microwave absorption of undoped, aluminized propellant flames is similar to that of doped propellants at pulsed field strengths investigated. However, at lower power levels (field strengths), it is expected that energy absorption to aluminum oxide features becomes more important. In addition to the ionic absorption of $NaNO_3$-doped flames, (2) aluminum oxide dipolar absorption can be significant, as indicated by the strong temperature dependence of the alumina loss tangent. The dielectric losses increase exponentially with increase in temperatures due to electron promotion to valence shells [23], [27]. At temperatures of 1500 K, aluminum oxide dielectric heating is 3000% more efficient than at room temperature, producing thermal runaway. The unaluminized AP propellant had a slightly lower absorption than aluminized doped and undoped propellants, which is expected to be a result of lower flame temperatures, absence of dopant, and absence of aluminum oxide which can absorb energy through dipole interactions.

Another mechanism for absorptions of microwave is condensed phase Maxwell-Wagner heating due to conductive spherical Al within a non-conductive matrix of AP and HTPB [19]. However, this is expected to be minimal based upon forward/reflected diode measurements conducted on an unignited propellant strand. Taken together, measurements indicate the microwave energy absorption of all the propellant formulations is high, indicating efficient energy deposition to a variety of propellant formulations can be achieved with pulsed, high peak power (field strength) microwave irradiation. It is expected that the various modes of energy absorption and doping are more important at lower field strength, as is indicated by previous results using continuous microwave irradiation [30].

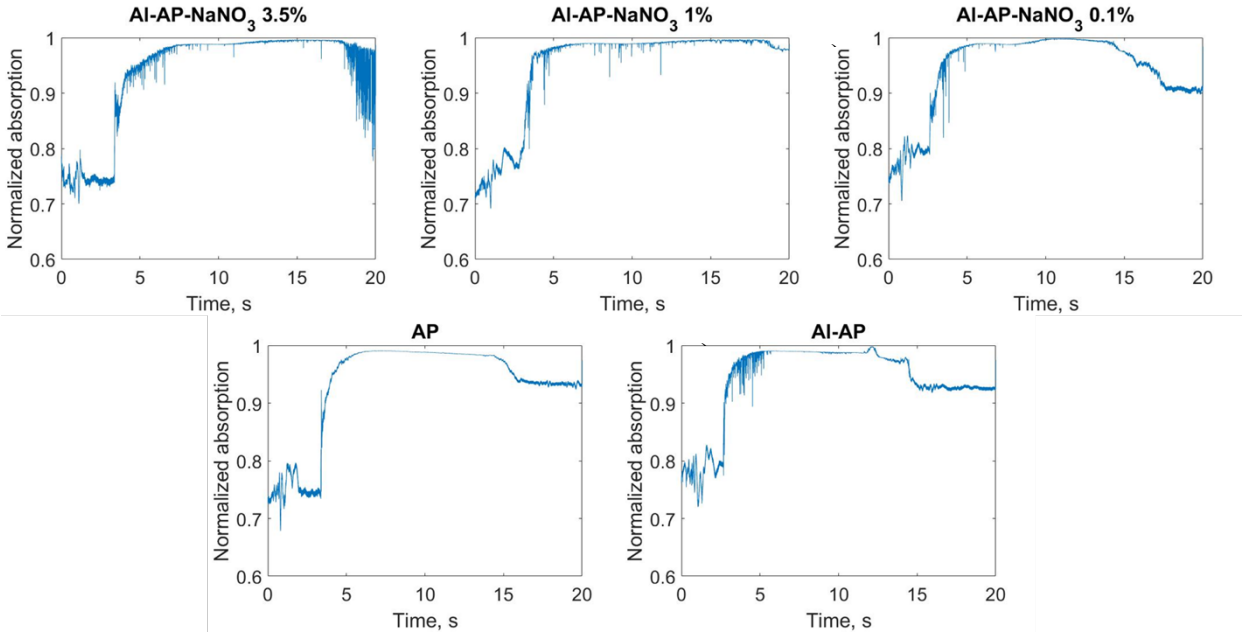

Fig. 10. *Normalized microwave power absorption measurements of burning composite propellants in the microwave cavity excited by a 30 kW peak power, 3 GHz field applied with 2 μs pulse duration and 0.001 duty cycle.*

5.4.2. Pulsed Microwave Energy Coupling and Relaxation

To explore the combustion environment before, during, and after field application, high-speed imaging of the pulse-microwave seeding within a composite propellant flame has been conducted using the same 2 μs duration pulse with 500 Hz (0.001 duty cycle). Some evidence exists suggesting enhancement events from subsequent 2 μs duration pulses are independent events, including the extinction of aforementioned high ionization charge shielding effects during subsequent microwave pulses as well as pulse-to-pulse similarity of the power absorption over a number of pulses. An image sequence of a typical pre- to post- enhancement environment (40,000 kHz, 10 μs exposure) of the burning surface of a piece of composite propellant is shown in Fig. 11. Pulsed field application is observed to result in significant and rapid growth of emission at the burning surface (0 to 25 μs) accompanied by enhanced emission from the reaction zone attached to the burning surface and extending ~2.5 cm. Significant relaxation of the enhanced zone occurs within 25 μs as evident by the lack of persistent emission, though it is unclear whether some near-surface enhancement persists at the location of enhancement. As flame structure at the burning surface of a composite propellant is highly heterogeneous, containing both premixed and diffusion flames as well as heating/igniting aluminum particles as well as oxide smoke from burning Al agglomerates, the source of the significant and rapid emission enhancement remains unclear, but will be explored through experimentation on propellants having varying flame feature length scales and composition. The similarity of emission during pre- and post-field application times indicates the unique ability of pulsed microwave fields to rapidly perturb the near-burning surface flame structure of a composite propellant. With regard to the effects of microsecond duration, high power fields on propellant burning rate, it was observed that a 30% burning rate enhancement can be achieved with application of 18 kW, 2 μs 1% duty cycle fields (3 GHz). With an average power of ~180 W, pulsed high field strength microwave irradiation can achieve a similar burning rate enhancement to CW microwave fields with roughly five times lower average power application.

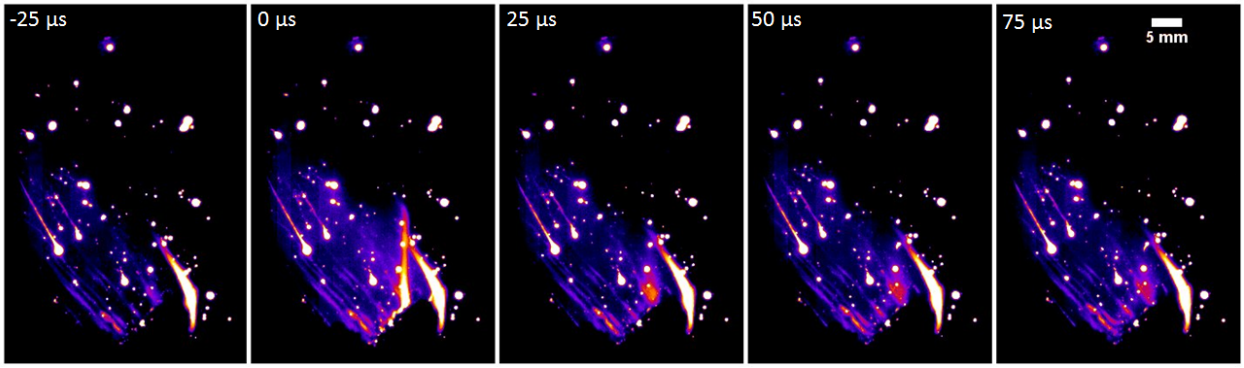

Fig. 11. *Image sequence showing microwave enhancement of the near-surface burning structure of an aluminized AP composite solid propellant by a 30 kW peak power, 2 µs, 500 Hz pulse of 3.00 GHz energy transmitted in a tuned resonant cavity. Application of the field occurs at approximately 0 µs. Frame rate and exposure duration are 40,000 kHz and 10 µs, respectively. False color is used to indicate emission intensity differences.*

5.5. AP Composite Propellant Dielectric Property Measurement

5.5.1. Measured Dielectric Properties

A summary of the results for all room-temperature data collected is given in Fig. 12. The transmission line method was collected continuously from 2.3 GHz to 2.65 GHz. The data overlays cAP $fNaNO_3$, BiAP $fNaNO_3$, and Teflon (standard), as a function of frequency. In the transmission line setup, Teflon measured real permittivities of 1.97 are within a 5% error of the actual value, [35] validating experimental configuration and analytical techniques. The average real and imaginary permittivities of CAP $fNaNO_3$ propellant articles is 5.83 and 0.228, respectively and average BiAP $fNaNO_3$ real and complex permittivities are 5.87 and 0.266 respectively. The loss tangent for both material is <<1, which is considered to be a low-loss medium and good dielectric. Furthermore, BiAP $fNaNO_3$ is more susceptible to microwave heating. This is expected to be a result of crystal interface. This is due to the number of interfaces within the bimodal AP propellant having more binder crystal interfaces. However this is a small difference between the two propellant dielectric properties, which changing the aluminum loading should change dielectric properties a considerably more [31].

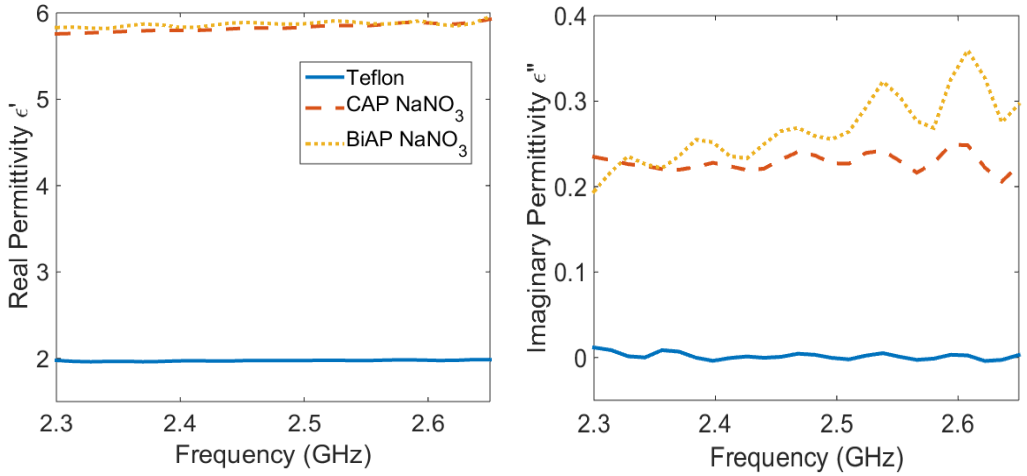

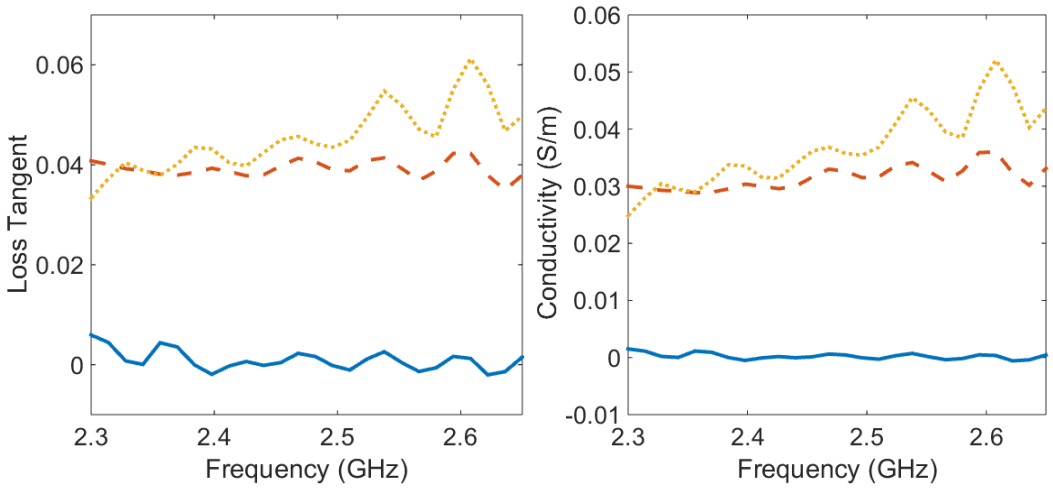

Fig. 12. *Graph of Teflon, CAP fNaNO₃, and BiAP fNaNO₃ real and imaginary permittivity, loss tangent, and conductivity as a function of frequency measured at room temperature.*

5.5.2. COMSOL Cavity Simulation

Initial COMSOL simulations of a loaded single-mode resonant microwave cavity operating at 2.45 GHz have been developed. This model will be modified by insertion of propellant strands having as-measured or modeled microwave properties. The cavity was designed to model the continuous microwave generator setup, seen in Fig. 13. In this setup, a 1 kW magnetron outputs into WR-284 waveguide to a Gerling Universal Applicator, with a quartz tube holder of OD 36mm. In this setup, propellant will be burnt under 2.45 GHz microwave field. To understand the field strength in the condense phase of this setup (preiginiton), a model with the quartz tube and propellant strand in the cavity and a model with the propellant strand and without the quartz tube is shown in Fig. 13. It is shown that field strength is ~40% lower with the quartz tube (36.3 kV/m) as compared to without the tube (59.1 kV/m). However in a propellant strand configuration, it is noted that burning propellant without a quartz tube is not feasible. COMSOL was also utilized to run RF heating of both types of propellants, in the same cavity. Results from this simulation can be seen in Table 4. As expected, bimodal AP fine $NaNO_3$ heating was greater due to its higher imaginary permittivity. Heating in a quartz tube and without in the waveguide of coarse AP fine $NaNO_3$ and bimodal AP fine $NaNO_3$ was 351.09 K and 394.16 K and, 358.73 K and 407.44 K respectively.

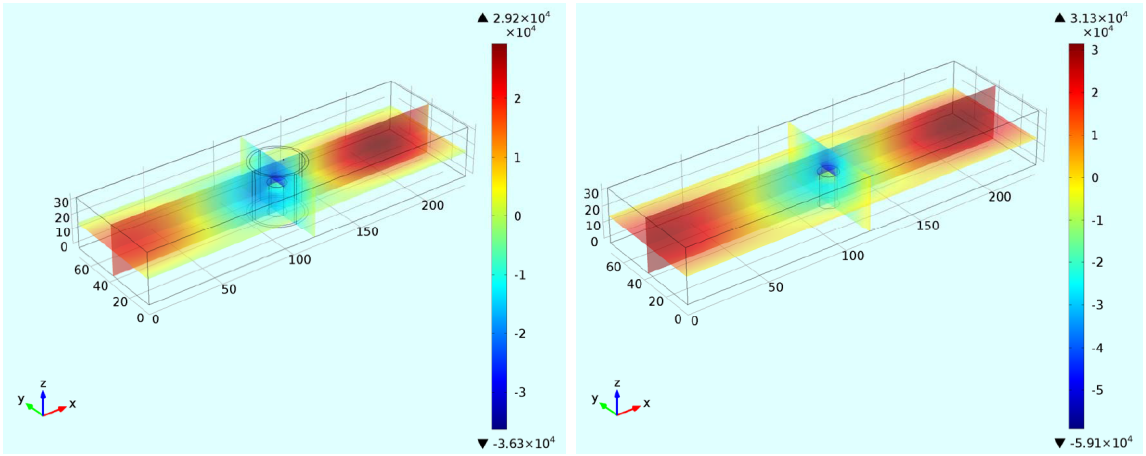

Fig. 13. *COMSOL simulation of propellant-loaded (BiAP fNaNO₃) single-mode resonant microwave cavity with 36 OD quartz tube (left) and without (right) quartz tube. Multiple slices show E-field strength (V/m) through the propellant center axis.*

Table 4. *Simulated loaded cavity reflection loss and isotropic, temperature-invariant heating times to heat propellant articles to an average temperature of 100 °C.*

	VSWR		Temperature in 20 (s) of Microwave Heating (K)	
Propellant	**No Quartz**	**Quartz Tube**	**No Quartz**	**Quartz Tube**
BiAP, fNaNO₃	1.229	2.259	407.44	358.73
cAP, fNaNO₃	1.226	2.256	394.16	351.09

6. Conclusions

This report describes the design and fabrication of atmospheric-pressure experimental apparatuses for study of microwave-energetic material flame interactions using both continuous-wave and pulsed microwave energy. Apparatuses are described and results are presented demonstrating the technique's ability to deposit energy to propellant flame structures in both continuous wave and pulsed microwave modes. The ability to measure the dielectric properties of composite sold propellants over discrete microwave wavelength bands is also demonstrated.

Specific to the effects of microwave radiation on energetic material flames, this effort explores the fundamental mechanisms of S-band microwave energy absorption of composite solid propellant flames. Specifically, the effort demonstrates the use of a small concentration of sodium nitrate dopant to form a microwave supported plasma within the composite propellant flame. Experimental results suggest that microwave irradiation of composite solid propellants result in microwave energy deposition by three mechanisms depicted in Fig. 1: (1) microwave supported plasma flame enhancement, (2) aluminum oxide thermal runaway dielectric loss, and (3) condensed phase propellant loss. Through variation of doping levels in atmospheric pressure combustion experiments, we demonstrate the beneficial effects of both aluminum combustion and addition of an alkali dopant on the ability enhance propellant flame structure and modulate the burning rate with application of microwave field. With ~38-91 kV/m, 2.46 GHz continuous fields

applied, absorption measurements suggest that 60-90% of microwave energy is absorbed by the flame structure and propellant condensed phase. Absorption measurements conducted on both burning and unburning propellants together suggest that ~20-30% of the total energy is absorbed by the flame structure, with the remainder being absorbed by the propellant condensed phase. Though less than half of the energy is absorbed by the flame, burning rate measurements suggest microwave-flame interactions are predominantly responsible for burning rate enhancements. We observe significant changes in the microwave-enhanced flame structure with addition of both sodium nitrate dopant and aluminum in the propellant composition. Microwave application to a propellant with up to 16% sodium nitrate dopant (replacement of AP) in a 15 wt. % aluminized AP composite propellant enables a 62% increase in burning rate. These results have significant implications on enhancement of metal combustion efficiency and on the ability to actively control energetic material combustion.

For pulsed microwave fields, this effort reports on the ability to rapidly perturb the combustion of an aluminized AP composite propellant using pulsed microwave field application to sodium nitrate-doped propellants which previously have been observed to exhibit flame temperature and burning rate enhancement under continuous S-band microwave irradiation. Measurements of forward and reflected power during application of 2 μs duration 30 kW fields suggest microwave energy absorption to the propellant flame is significant for all formulations. High-speed imaging during pulse applications demonstrates energy deposition occurs rapidly near/at the propellant burning surface as indicated by significant gas phase emission enhancement. Emission relaxation of plasma events occurs rapidly, with little residual emission enhancement observed after 25 μs. More experiments are required to investigate near burning surface combustion enhancement mechanisms and pulse/post-pulse thermal environments; these measurements are particularly challenging given the short duration of the field application event and the plasma formation/quench timescales. With respect to propulsion devices, pulse techniques may hold promise to enable dynamic enhancement and control of motor thrust, burning rate, and combustion stabilization.

This work has demonstrated the ability to measure dielectric properties of a sodium nitrate-doped, aluminized, AP composite propellant. It has been demonstrated that two different formulation, coarse AP fine $NaNO_3$ and bimodal AP fine $NaNO_3$ are low lossy, good dielectric materials in the condensed phase. Furthermore, a COMSOL model was develop to understand the electric field strength in a continuous microwave cavity, based off from an experiment and E-fields were reported. Additional efforts will focus on discovering the effects of particle loading of aluminum in dielectric properties of propellants. Furthermore, particle size of aluminum will be investigate and a model will be developed to pull out dielectric properties for a numerous variation of propellants. With this knowledge, we can develop a model of perforated motor design to be tuned and impedance match as a transient function of geometry changes. With this knowledge, effective tuning and design of a motor will be considered to optimize microwave energy enhancement.

7. References

[1] S. R. Chakravarthy, J. M. Seitzman, E. W. Price, and R. K. Sigman, "Intermittent Burning of Ammonium Perchlorate–Hydrocarbon Binder Monomodal Matrixes, Sandwiches, and Propellants," *J. Propuls. Power*, vol. 20, no. 1, 2004.

[2] T. Parr and D. Hanson-Parr, "Optical Diagonsitcs of Solid-Propellant Flame Structure," in *Solid Propellant Chemistry, Combustion, and Motor Interior Ballistics*, V. Yang, T. B. Brill, and W.-Z. Ren, Eds. Reston, VA: AIAA, 2000, pp. 381–441.

[3] F. E. . Culick, *Unsteady Motions in Combustion Chambers for Propulsion Systems,* Mouvements instables dans les chambres, vol. 323, no. December. 2006.

[4] W. N. Sawka, A. Katzakian, and C. Grix, "Solid State Digital Propulsion Cluster Thrusters For Small Satellites, Using High Performance Electrically Controlled Extinguishable Solid Propellants," in *19th Annual AIAA/USU Conference on Small Satellites*, 2005.

[5] J. Li, T. Litzinger, and S. Thynell, "Plasma Ignition and Combustion of JA2 Propellant," *J. Propuls. Power*, vol. 21, no. 1, pp. 44–53, 2005.

[6] J. Li, T. Litzinger, M. Das, and S. Thynell, "Recombination of Electrothermal Plasma and Decomposition of Plasma-Exposed Propellants," *J. Propuls. Power*, vol. 22, no. 6, pp. 1353–1361, 2006.

[7] X. Li, R. Li, S. Jia, and Y. Zhang, "Interaction features of different propellants under plasma impingement," *J. Appl. Phys.*, vol. 112, no. 63303, 2012.

[8] R. Alimi and V. Berdichevsky, "Mechanism of solid propellant combustion submitted to a high plasma flux," *Propellants, Explos. Pyrotech.*, vol. 33, no. 2, pp. 118–121, 2008.

[9] A. J. Porwitzky, L. C. Scalabrin, M. Keidar, and I. D. Boyd, "Chemically Reacting Plasma Jet Expansion Simulation for Application to Electrothermal Chemical Guns," in *38th AIAA Plasmadynamics and Lasers Conference*, 2007, pp. 1–17.

[10] K. Hasue, M. Tanabe, N. Watanabe, S. Nakahara, F. Okada, and A. Iwama, "Initiation of some energetic materials by microwave heating," *Propellants, Explos. Pyrotech.*, vol. 15, no. 5, pp. 181–186, 1990.

[11] M. E. Daily, B. B. Glover, S. F. Son, and L. J. Groven, "X-band microwave properties and ignition predictions of neat explosives," *Propellants, Explos. Pyrotech.*, vol. 38, no. 6, pp. 810–817, 2013.

[12] A. Starikovskiy, "Physics and chemistry of plasma-assisted combustion," *Philos. Trans. R. Soc. London A Math. Phys. Eng. Sci.*, vol. 373, no. 2048, 2015.

[13] Y. Ju and W. Sun, "Plasma assisted combustion: Dynamics and chemistry," *Prog. Energy Combust. Sci.*, vol. 48, pp. 21–83, 2015.

[14] J. B. Michael, A. Dogariu, M. N. Shneider, and R. B. Miles, "Subcritical microwave coupling to femtosecond and picosecond laser ionization for localized, multipoint ignition of methane/air mixtures," *J. Appl. Phys.*, vol. 108, no. 9, 2010.

[15] S. Popović, R. J. Exton, and G. C. Herring, "Transition from diffuse to filamentary domain in a microwave-induced surface discharge Transition from diffuse to filamentary domain in a 9.5 GHz microwave-induced surface discharge," *Appl. Phys. Lett*, vol. 87, no. 61502, 2005.

[16] I. I. Esakov, L. P. Grachev, K. V Khodataev, V. L. Bychkov, and D. M. Van Wie, "Surface Discharge in a Microwave Beam," *IEEE Trans. Plasma Sci.*, vol. 35, no. 6, pp. 1658–1663, 2007.

[17] P. F. Barker, B. McAndrew, S. O. Macheret, and R. B. Miles, "Control of sub-critical

microwave filamentary plasma in dense gases," in *Plasma Science, 2000. ICOPS 2000. IEEE Conference Record-Abstracts. The 27th IEEE International Conference on*, 2000, p. 158.

[18] J. B. Michael, T. L. Chng, and R. B. Miles, "Sustained propagation of ultra-lean methane/air flames with pulsed microwave energy deposition," *Combust. Flame*, vol. 160, no. 4, pp. 796–807, 2013.

[19] A. C. Metaxas and R. J. Meredith, "Industrial Microwave Heating," *Peter Peregrinus Ltd.*, vol. 29, no. 9, London, p. 659, 1983.

[20] S. Gordon and B. J. McBride, *Computer Program for Calculation Complex Chemical Equilibrium Compositions and Applications*, 1994.

[21] J. E. Gerling, "Journal of Microwave Power and Electromagnetic Energy Microwave Oven Power: A Technical Review Microwave Oven. Power: A Technical Review," *J. Microw. Power Electromagn. Energy*, vol. 224, pp. 199–207, 1987.

[22] W. E. Price, "Combustion of Metalized Propellants," in *Fundamentals of Solid-Propellant Combustion*, K. Kuo, Ed. New York: AIAA, 1984, pp. 479–513.

[23] W. H. Sutton, "Microwave processing of ceramic materials," *Am. Ceram. Soc. Bull.*, vol. 68, pp. 376–386, 1989.

[24] H. J. Kitchen *et al.*, "Modern microwave methods in solid-state inorganic materials chemistry: From fundamentals to manufacturing," *Chemical Reviews*, vol. 114, no. 2. pp. 1170–1206, 2014.

[25] B. C. Terry, Y. C. Lin, K. V. Manukyan, A. S. Mukasyan, S. F. Son, and L. J. Groven, "The effect of silicon powder characteristics on the combustion of silicon/teflon/viton nanoenergetics," *Propellants, Explos. Pyrotech.*, vol. 39, no. 3, pp. 337–347, 2014.

[26] K. Möllmann, F. Pinno, and M. Vollmer, "Two-Color or Ratio Thermal Imaging – Potentials and Limits," *FLIR Tech. Ser.*, pp. 1–13, 2010.

[27] V. M. Kenkre, L. Skala, M. W. Weiser, and J. D. Katz, "Theory of microwave interactions in ceramic materials: the phenomenon of thermal runaway," *J. Mater. Sci.*, vol. 26, no. 9, pp. 2483–2489, 1991.

[28] E. C. Koch, *Metal Fluorocarbon Based Energetic Materials*, Wiley, New York, 2012.

[29] S. Bastea *et al.*, "Cheetah 8.0 User Manual," *Lawrence Livermore Natl. Lab. Energ. Mater. Cent.*, 2015.

[30] J. Lynch, M. Ballestero, S. Barkley, R. Cazin, J. B. Michael, and T. R. Sippel, "Microwave-supported plasma combustion enhancement of composite solid propellants using alkali metal dopants," in *54th AIAA Aerospace Sciences Meeting*, 2016.

[31] Y. S. Ho and J. J. Kramer, "Microwave Dielectric Properties of Metal Filled Particulate Composites," in *Materials Research Society Symposia Proceedings*, 1988, vol. 124, pp. 161–166.

[32] W. L. Perry, D. W. Cooke, J. D. Katz, and A. K. Datye, "On the possibility of a significant temperature gradient in supported metal catalysts subjected to microwave heating," *Catal. Letters*, vol. 47, no. 1, pp. 1–4, Aug. 1997.

[33] A. L. Higginbotham Duque, W. L. Perry, and C. M. Anderson Cook, "Complex Microwave Permittivity of Secondary High Explosives," *Propellants Explos. Pyrotech.*, vol. 39, no. 2, pp. 275–283, 2014.